The Hydrosphere

Lecture 04

Water-rock interaction will come later

The isotope water cycle

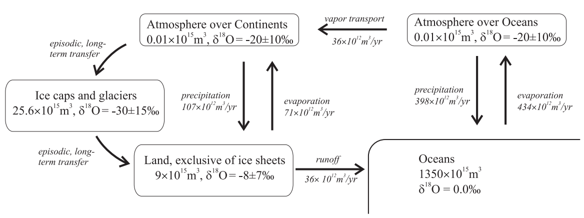

Global Meteoric Water Line

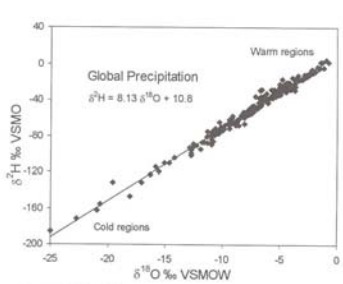

Fig. 2-1 The meteoric relationship for ^{18}O and ^{2}H in precipitation. Data are weighted average annual values for precipitation monitored at stations in the IAEA global network, compiled in Rozanski et al. (1993).

Evaporation

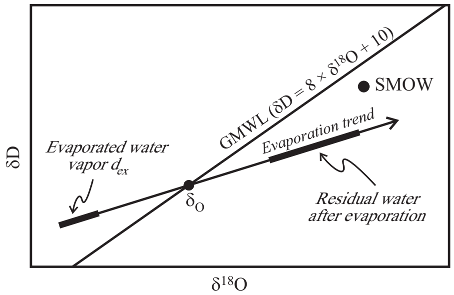

Evaporation of small reservoir

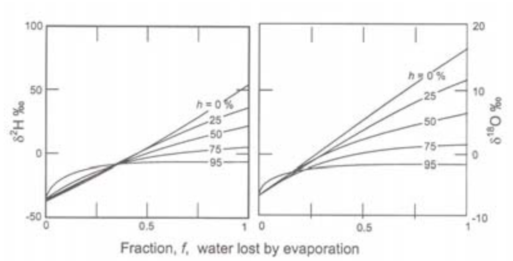

Fig. 2-23 The isotopic composition of lake water for varying fractions of water loss by evaporation, assuming well mixed conditions and constant volume (inflow = outflow + evaporation). For $f = 1$ evaporation = inflow and no outflow exists. Calculations are made for various relative humidities (from Gonfiantini, 1986).

Evaporation of finite reservoir

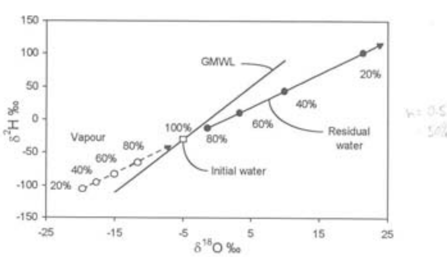

Fig. 2-9 Isotopic evolution of a finite volume of water during evaporation with 50% humidity. Solid points are the residual water at given percentages of the initial reservoir. Open points are the isotopic composition of the accumulating vapour reservoir. The vapour is initially depleted, but evolves toward the isotopic composition of the initial water.

Evaporation of infinite reservoir

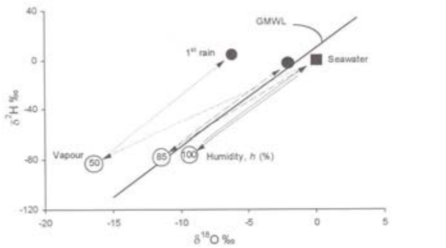

Fig. 2-10 Kinetic isotope effects during evaporation of seawater to form vapour (open circles with *h* in %) for various humidities at 25°C, together with the 1st rain (filled circles) formed by equilibrium condensation. When humidity is less than 100% excess deuterium is found in the rain.

Evaporation slopes

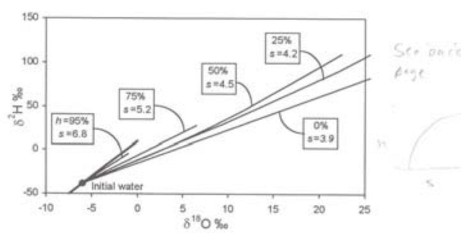

Fig. 2-8 Isotopic enrichment in evaporating water and the effect of humidity. Slopes are approximations of early portion of each curve near the GMWL (heavy line) (from Gonfiantini, 1986).

Deuterium excess and relative humidity

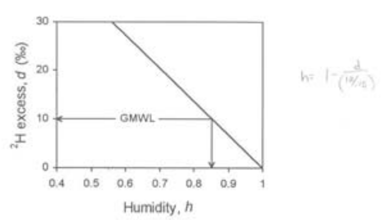

Fig. 2-11 The deuterium excess parameter, *d*, as a function of humidity, *h*, during kinetic evaporation from the ocean surface. Only a minor variation in *d* occurs with a change in temperature (after Merlivat and Jouzel, 1979).

Local Meteoric Water Lines

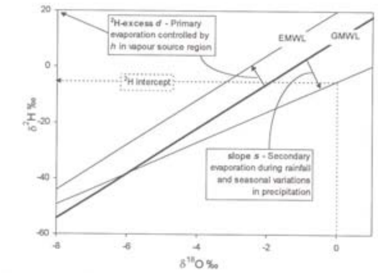

Fig. 2-18 Principal factors affecting the slope *s* and deuterium excess *d* of meteoric water lines. Note the distinction between deuterium excess, which is calculated for a slope of 8, and the deuterium intercept, determined with the actual slope and for $\delta^{18}O = 0$.

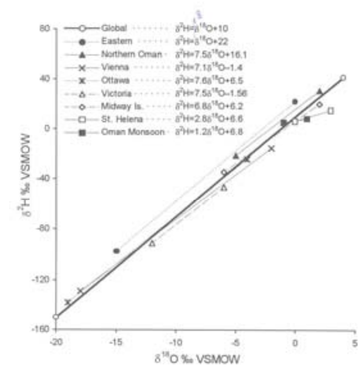

1-20 Regional and local meteoric water lines from various weather stations (Global — Craig, 1961a; Eastern — Gat and ..., 1970; Victoria, Ottawa — Fritz et al., 1987a; Vienna, Midway Is., St. Helena — Rozanski et al., 1993; Oman — ..., 1987).

Rayleigh Distillation

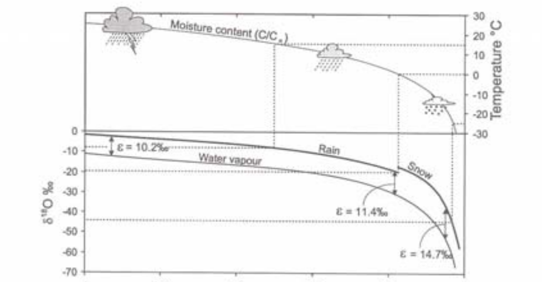

Fig. 2-13 The change in the ^{18}O content of rainfall according to a Rayleigh distillation, starting with $\delta^{18}O_{vapour} = -11‰$, temperature = 25°C, and a final temperature of −30°C. Note that at 0°C, fractionation between snow and water vapour replaces rain-vapour fractionation. The fraction remaining has been calculated from the decrease in moisture carrying capacity of air at lower temperatures, starting at 25°C (from calculations for Fig. 2-4). Dashed lines link $\delta^{18}O$ of precipitation with temperature of condensation.

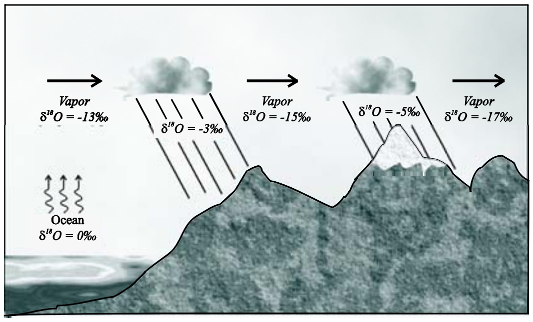

GLOBAL NETWORK OF ISOTOPES IN PRECIPITATION

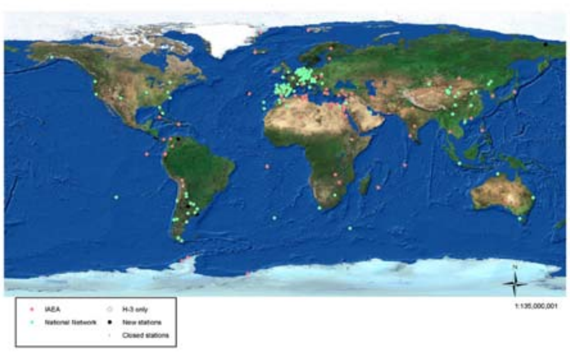

Global Distribution

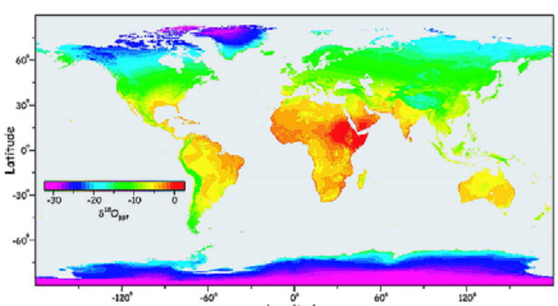

Bowen, G.J. and Wilkinson, B., 2002. Spatial distribution of delta O-18 in meteoric precipitation. Geology, 30(4): 315-318.

Temperature Effect

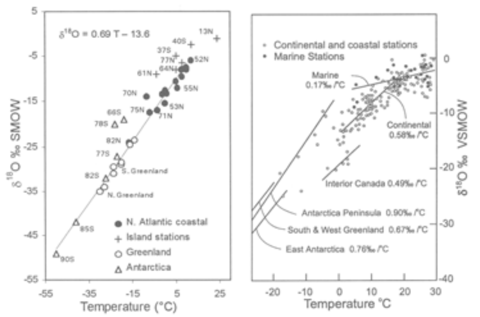

Fig. 3-1 The global T–$\delta^{18}O$ relationship for precipitation, modified from Dansgaard, 1964 (left). Temperature is mean annual air temperature (MAAT) at the station. Data from the extensive IAEA Global Network for Isotopes in Precipitation (GNIP) shows this relationship to be a combination of regional T–$\delta^{18}O$ lines, with strong differences between marine, continental and interior stations, from Rozanski et al., 1993 (diagram on right).

Continental effect

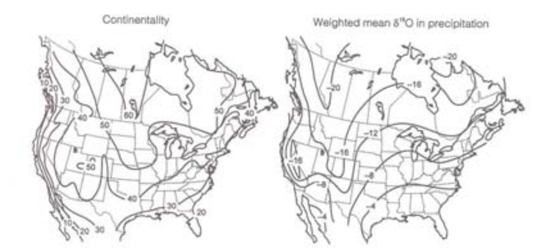

Fig. 3-3 Isopleths of continentality for North America calculated using Conrad's index (modified from Barry and Chorley, 1987) compared with the weighted mean-annual $\delta^{18}O$ composition of precipitation (IAEA GNIP data). The index of continentality is based on seasonal extremes in temperature and latitude. Patterns of $\delta^{18}O$ reflect continentality at this scale, although deviations occur in the north central regions due to seasonal biases in precipitation.

Continental effect

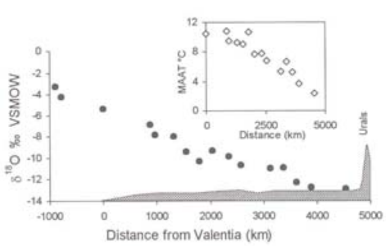

Fig. 3-4 The evolution of $\delta^{18}O$ in precipitation over the low-relief European continental margin from the Atlantic Weathership station, through Valencia on the southwest coast of Ireland to Perm near the Ural Mountains. Data are long-term average annual ^{18}O content of precipitation for European stations (modified from Rozanski et al., 1993). Inset shows the near-linear correlation of mean annual air temperature (MAAT) along this trajectory.

Altitude effect

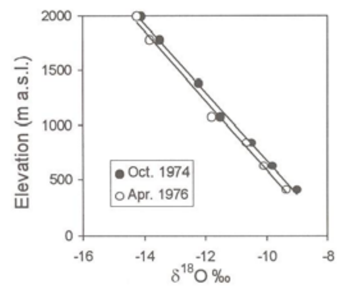

Fig. 3-6 The relationship between altitude and $\delta^{18}O$ in precipitation in Val Corsaglia, maritime piedmont of the Italian Alps (Bortolami, 1979). Samples were collected in October 1974 and April 1976, representing months of the fall and spring seasons with similar mean monthly temperatures. The mean gradient for these data is −0.31 ‰ $\delta^{18}O$ per 100-m rise.

Altitude effect

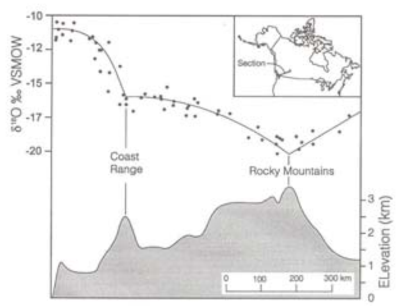

Fig. 3-5 The evolution of $\delta^{18}O$ in precipitation across the high-relief continental margin of the Canadian Cordillera, from the Pacific Ocean to the interior plains of Alberta (profile line shown on inset) (modified from Yonge et al., 1989). Decreasing T with distance and altitude along the trajectory drives rainout and depletion of ^{18}O.

Altitude gradients

Site	*Region*	*Altitude (m asl)*	*Gradient (‰ per 100 m)* $\delta^{18}O$	$\delta^{2}H$	*Reference*
Jura Mountains	Switzerland	500-1200	−0.2		Siegenthaler et al.,, 1983
Black Forest	Switzerland	250-1250	−0.19		Dubois and Flück, 1984
Mont Blanc	France	2000-5000	−0.5*	−4	Moser and Stichler, 1970
Coast Mountains	British Columbia	250-3250	−0.25		Clark et al., 1982
Piedmont	Western Italy	500-2000	−0.31	−2.5	Bortolami, 1979
Dhofar Monsoon	Southern Oman	0-800	−0.10		Clark, 1987
Saiq Plateau	Northern Oman	400-2000	−0.20		Stanger, 1986
Mount Cameroun	West Africa	0-4095	−0.155		Fontes et al., 1977

* Calculated from $\delta^{2}H$ using a slope of 8.

Amount effect

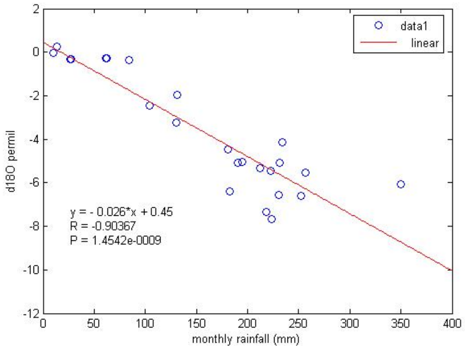

Source effect

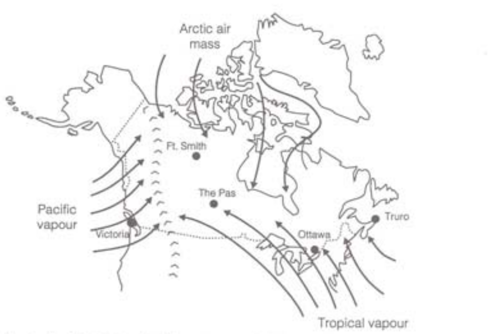

Fig. 2-19 Meteoric regimes in Canada. The effect of these systems on precipitation is seen in the local meteoric water lines for stations across the country. The Arctic air stream brings no moisture, except locally in the north during summer.

Seasonal effect

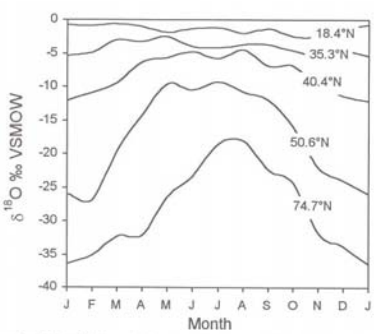

Fig. 3-8 The seasonal variation in $\delta^{18}O$ in precipitation at stations from low to high latitude in North America. Data are for monthly averages at San Juan, Puerto Rico (18.4°N), Cape Hatteras, North Carolina (35.3°N), Coshocton, Ohio (40.4°N), Gimli, Manitoba (50.6°N), and Resolute, NWT (74.7°N).

Seasonal/Source effect at ABQ